ORIGINAL RESEARCH

Radiation dosimetry of [11C]TZ1964B as determined by whole-body PET imaging of nonhuman primates

Baijayanta Maiti[1,2]*, Noah L. Goldman[1], Mahdjoub Hamdi[2], Jason Lenox-Krug[1], Morvarid Karimi[1], Stephen M. Moerlein[2], Richard Laforest[2], Tianyu Huang[2], Zhude Tu[1,2], Joel S. Perlmutter[1,2,3,4,5] and Scott A. Norris[1,2]

Abstract

Background Phosphodiesterase 10A (PDE10A) is a postsynaptic, membrane bound cyclic nucleotide phosphodiesterase that is highly enriched in the striatal medium spiny neurons and regulates dopaminergic neurotransmission. The objective of this study is to determine the absorbed radiation dosimetry of a novel radiotracer for PDE10A: 3-(Methoxy-11C)-2-((4-(1-methyl-4-(pyridine-4yl)-1*H*-pyrazol-3-yl)phenoxy)methyl)quinolone ([11C]TZ1964B) based on whole body PET imaging in nonhuman primates, a critical step before translating this radiotracer to imaging studies in humans. [11C]TZ1964B may contribute to the clinical investigation of multiple neuropsychiatric conditions including Parkinson disease, Huntington disease and schizophrenia. For absorbed radiation measures, two males and one female cynomolgus monkeys (*Macaca fascicularis*) had intravenous injections of 302.3–384.4 MBq of [11C]TZ1964B followed by sequential whole body PET imaging in a MicroPET-Focus220 scanner. Volumes of interest (VOIs) that either encompassed the entire organ or sampled regions of highest activity within larger organs were defined. Time-activity curves were derived from the PET data for each VOI, and analytical integration of its multi-exponential fit yielded the organ time-integrated activity. We generated human radiation dose estimates based on the scaled organ residence using OLINDA/EXM2.2.

Results Highest retention was observed in the liver with total time-integrated activity of ~0.23 h. Absorbed organ dosimetry was highest in the liver (53.3 µGy/MBq), making it the critical organ. Gallbladder (35.9 µGy/MBq) and spleen (35.4 µGy/MBq) were the next highest organs for absorbed radiation dose. Effective doses were estimated to be 5.02 and 5.84 µSv/MBq for males and females, respectively.

Conclusions This nonhuman primate dosimetry study suggests intravenous doses up to 938 MBq of [11C]TZ1964B can be safely administered to human subjects for PET measurements of PDE10A activity. The tracer kinetic data is consistent with a hepatobiliary clearance pathway for the radiotracer.

Keywords [11C]TZ1964B, PDE10A, Dosimetry, PET

*Correspondence:
Baijayanta Maiti
maitib@wustl.edu
Full list of author information is available at the end of the article

Maiti *et al. EJNMMI Research*   (2025) 15:57

Page 2 of 9

Background

Phosphodiesterase 10A (PDE10A) is a postsynaptic, membrane bound, dual-substrate specific cyclic nucleotide phosphodiesterase that is highly enriched in striatal medium spiny neurons (MSNs) [1, 2]. Dopaminergic (DA) neurotransmission is mediated by the differential activation of the downstream cAMP/protein kinase A (PKA) signaling cascade [3]. DA stimulation of D1-like receptors on MSNs constituting the direct pathway upregulates cAMP/PKA signaling via activation of adenylyl cyclase with enhanced production of cAMP [3]. On the contrary, DA stimulation of MSNs expressing D2-like receptors (indirect pathway) downregulates cAMP/PKA signaling pathway.

PDE10A catalyzes hydrolysis of cAMP in striatal neurons and thereby regulates dopaminergic signal transduction by suppressing downstream cAMP/PKA signaling cascades [1]. Thus, PDE10A plays a key role in basal ganglia function and is likely involved in the pathophysiology of disorders involving the basal ganglia such as Parkinson disease, Huntington disease, obsessive compulsive disorder and schizophrenia [4–7]. This highlights the potential role of PDE10A radiotracers as in vivo biomarkers of striatal function and nigrostriatal injury, as a biomarker of disease progression and as a metric of target engagement for novel disease modifying therapies for these conditions. One other PDE10A PET radiotracer [18F]MNI-659, with different pharmacokinetics has been used in clinical research but not yet been applied for routine clinical work, highlighting the urgent need for the development of novel radiotracers [8, 9].

Several recently tested PET radioligands for PDE10A demonstrate potent binding affinity and good selectivity for PDE10A, but several of them have nonpolar metabolites [10–12] that could cross the blood brain barrier rendering them suboptimal for human studies. The radioligand [11C]TZ1964B, which contains a methoxy group on its quinoline fragment demonstrates high affinity and selectivity for binding to the PDE10A isoform [13–16]. This radioligand has a slow in vivo peripheral metabolism profile and the formation of only a single hydrophilic radiometabolite. After intravenous injection, [11C]TZ1964B has high blood brain barrier penetration, selective striatal uptake and relatively rapid clearance, which is potentially advantageous for PET studies of drugs [16]. Some other PDE10A radioligands like [18F]MNI-659 or [11C]T-773 also do not have hydrophobic radiometabolites [17, 18]. Comparative analyses utilizing double scans in the same monkey using both [18F]MNI-659 and [11C]TZ1964B demonstrated the suitability of both as PET radiotracers for brain PDE10A levels but each had unique traits in addition to their contrasting half-lives: [11C]TZ1964B had higher striatal retention enabling better measurements for static scan acquisition, steady-state analysis methods or for displacement studies whereas [18F]MNI-659 demonstrated higher initial tracer uptake but faster washout (similar to [11C]T-773) and hence would be better suited for short-term dynamic scans or dissociation rates measurements [16]. Additionally, the short half-life of 11C-labeled tracer (unlike 18F) permits multiple PET scans that can be useful for displacement or intervention studies in a single imaging session.

The objective of this study is to estimate the human radiation dosimetry [11C]TZ1964B based on extrapolation from PET data obtained after intravenous injection of the radiotracer into nonhuman primates and sequential whole-body PET scanning. These preclinical radiation dose measurements enable estimation of safe administration doses of [11C]TZ1964B for first-in-human PET studies.

Methods

Radiopharmaceutical preparation

[11C]TZ1964B (3-(Methoxy-11C)-2-((4-(1-methyl-4-(pyridine-4yl)-1*H*-pyrazol-3-yl)phenoxy)methyl)quinolone) was prepared in a Good Laboratory Practice (GLP) facility as previously described [13]. Briefly, $^{11}CO_2$ was converted to [11C]CH_3I (methyl iodide) using a PETtrace MeI MicroLab (GE Medical Systems, Milwaukee, WI, USA) module and immediately utilized for the O-methylation of the quinoline precursor. The reaction mixture was purified by reverse phase high-performance liquid chromatography (HPLC), and the product sterilized by membrane filtration (0.2 μm) in a reformulation solution of 10% ethanol in 0.9% Sodium Chloride Injection, USP. The steps involving the synthesis of the cold standard, precursor and the radiosynthesis of [11C]TZ1964B were in accordance with our previously published protocol [13, 14]; further detailed in Supplementary data (Scheme 1 and Figs. 1s and 2s). Quality control testing verified product radiochemical purity was > 99% and specific activity was > 204 GBq/μmol (decay-corrected to end-of-synthesis).

Nonhuman primate subjects

Two males and one female cynomolgus monkeys (*Macaca fascicularis*) underwent whole-body PET scanning for the dosimetry analyses as previously described [15, 19, 20]. The macaques were fasted overnight prior to each scan. Ketamine (10 mg/kg, intramuscular) was administered to induce anesthesia in conjunction with intramuscular glycopyrrolate to reduce secretions. Ondansetron was administered on an as-needed basis for emesis; only the female monkey
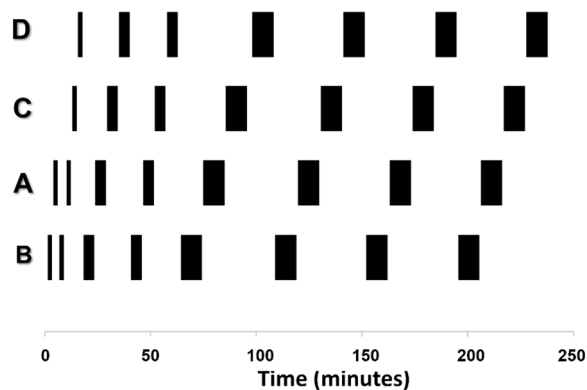
Maiti *et al. EJNMMI Research* (2025) 15:57

Page 3 of 9

Fig. 1 Outline of scanning sequence: Seven to eight successive PET scans of increasing duration were obtained to cover A (whole brain), B (heart and lungs), C (liver, gallbladder and kidneys), and D (urinary bladder, small and large intestines)

required ondansetron during the second scan due to emesis after induction of anesthesia. A 20-gauge plastic catheter was inserted into a limb vein for radiotracer injection; soft-cuffed endotracheal tube was inserted into trachea for mechanical ventilation; and isoflurane was used for maintenance of anesthesia. Surgical tape firmly secured the head position; water soluble ophthalmic ointment was applied to the eyes to protect the corneas, and the eyelids were taped shut. The body temperature was maintained at ~37° C with a heated water blanket. Vitals including heart rate, end-tidal PCO_2 and rectal temperature were monitored continuously during the scans.

We used the minimum number of animals necessary for this study, and in accordance with the recommendations of the Weatherall report "The use of non-human primates in research," all steps were taken to ameliorate suffering. Guidelines prescribed by the National Institutes of Health (NIH) Guide for the Care and Use of Laboratory Animal were followed at all times, and this work had the approval the Institutional Animal Care and Use Committee (IACUC; study numbers: 20150166 and 20180143) of Washington University in St. Louis. All animals were housed individually; maintained in facilities with 12-h dark and light cycles; provided access to food and water ad libitum; and were equally engaged with a variety of psychologically-enriching tasks, such as watching movies or playing with appropriate toys.

PET data acquisition

PET images were acquired using a Siemens MicroPET-Focus 220 scanner (Concorde/CTI/Siemens Microsystems, Knoxville, TN). The automated transaxial positioning of the scanning bed within 0.2 mm tolerances enabled sequential repositioning of the monkeys within the scanner; the sequence and duration of acquisition in each position is delineated in Fig. 1 and Table 1s. Four 30-min-long transmission scans with Co-57 point source were acquired in four different positions immediately prior to the injection of the radioligand for attenuation correction measurements. The assigned sections (and organs included therein) were A (whole brain), B (heart and lungs) C (liver, gallbladder and kidneys) and D (urinary bladder, small and large intestines). Biodistribution data was collected from sequential whole body PET images starting immediately after bolus injection (administered over 30 s followed immediately by a saline flush)
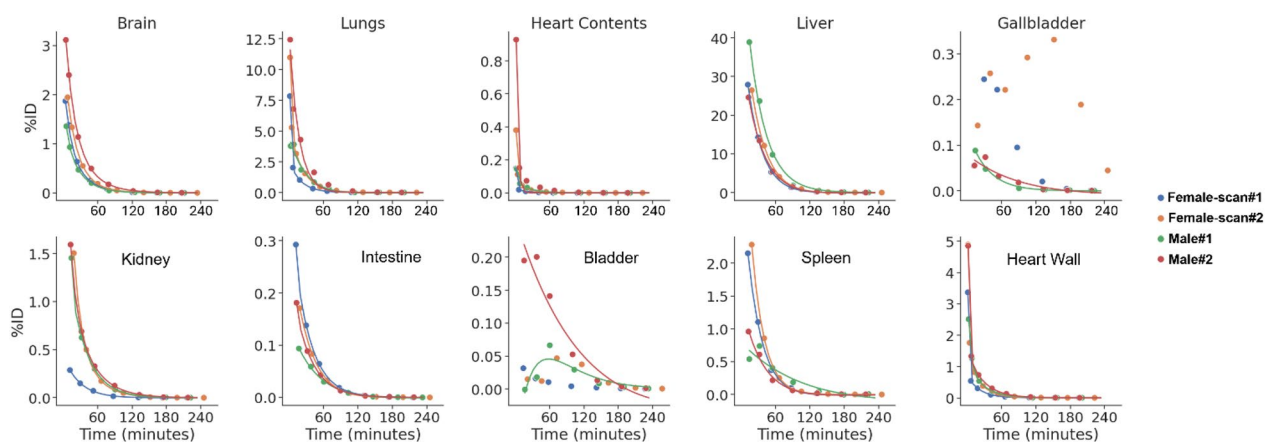

Fig. 2 Time-activity curves with activity expressed in percentage of injected dose per organ. The non-decay corrected representative organ time-activity curves from scans in the two male macaques and from two scan sessions obtained 3 years apart in the same female macaque are shown here. Area under the curve for bladder and gallbladder uptake from scan#1 and scan#2 from the female monkey had a poor exponential fit and were integrated using the trapezoid method

Table 1 Approximate in vivo biodistribution of radioactivity following intravenous injection of [^{11}C]TZ1964B

Organ	Percent injected dose per organ (%)[a]			
	Scan Time (21 ± 12 min)[b]		Scan Time (70 ± 23 min)[b]	
	Average	SD	Average	SD
Brain	1.70	0.54	0.327	0.12
Heart wall	1.12	0.49	0.180	0.16
Heart contents	0.086	0.08	0.014	0.05
Lungs	4.20	2.00	0.87	0.62
Liver	18.4	4.61	1.69	0.27
Kidneys	0.62	0.28	0.09	0.04
Gallbladder	0.151	0.09	0.091	0.09
Bladder	0.06	0.08	0.04	0.02
Intestine	0.107	0.025	0.015	0.002
Spleen	0.98	0.30	0.114	0.045

[a] Includes radioactivity in blood compartment. The two columns of data refer to two separate scanning intervals

[b] Mean and standard deviation for the measurement times for four experiments

of [^{11}C]TZ1964B with 7–8 successive scans spanning each of the above four body sections (Fig. 1).

The two male monkeys weighed 8.6 kg and 6.8 kg and received 302.3 MBq and 336.3 MBq of [^{11}C]TZ1964B, respectively. The female monkey underwent the injection and scan procedure twice on non-consecutive days; it weighed 6.9 kg and 7.8 kg and received 342.3 MBq and 384.4 MBq of radiotracer [^{11}C]TZ1964B for each independent scan session.

Data analysis

Scans were reconstructed using filtered back projection with a ramp filter at Nyquist frequency along with corrections for attenuation, scatter, random and dead time. The reconstructed image resolution was < 2.0 mm full width half maximum for all three dimensions at the center of the field of view. PET image counts were calibrated to a dose calibrator to convert measured PET uptake to microcuries of ^{11}C.

All organs with discernible accumulation of radioactivity were included for image quantification using two distinct approaches. For some organs, volumes of interest (VOI s) encompassing the entire organ (brain, and heart) were drawn using ASIPro VM™ MicroPET analysis software (Siemens PreClinical Solutions, Knoxville TN). We also traced a VOI specifically for the heart chambers (described henceforth as "Heart contents"); subtraction of the uptake of this VOI from the VOI encompassing the entire heart generated the measures for the heart wall. In other cases, where a single comprehensive VOI greater than the entire organ

(lungs, liver, gallbladder, spleen, kidney, urinary bladder and intestine) could not be reliably defined to ascertain an accurate estimation of the radioactivity uptake of the whole organ, an alternate approach was pursued. Several small representative VOIs that included regions with the highest radioactivity accumulation within the target organ were chosen; the average radioactivity concentration across all the VOIs for a specific organ multiplied by the entire organ weight generated a liberal estimate of absorbed radioactivity within the whole organ. This approach likely overestimates the organ dosage given the assumption that areas of nonselective accumulation within the organ have the same uptake of radioactivity as those regions with selective accumulation.

The PET-based regional radioactivity measurements were used to determine the percentage of injected dose per organ (%ID/organ); standard organ volumes were normalized to each animal's body weight. The calculated radioactivity in the entire organ was plotted as a function of time to construct the organ time-activity curves. Time-integrated activity calculations for each organ were obtained by the analytical integration of the multi-exponential fit with two exponentials on the non-decay corrected time-activity curves. The area under the curve for a few organs (bladder and gallbladder from both scans in the female monkey) with a poor exponential fit were integrated using the trapezoid method to generate the residence times; the activities after the last frame in such cases were ignored as the total PET measurements spread out to almost 12 half-lives of this ^{11}C-labeled tracer and there was very little to no remnant activity at this time point. The time-integrated activity assigned to the remainder-of-body (maximal theoretical residence time for ^{11}C minus the sum of the measured time-integrated activity) comprised blood activity that was not specifically assigned to an organ and "missing" activity not accounted for in the sampled organs. No loss of urine or fecal matter was noted following injection of the radioligand during any of the PET data acquisition sessions reported here.

The calculated time-integrated activity was scaled using the equation: scaled T(human) = T(animal) x [(M_organ (human))/(M_total (human))]/ [(M_organ (animal))/(M_total (animal))] as previously described [20] where T implies time-integrated activity and M_organ and M_total represent individual organ weight and total body weight respectively. Percentage body weights of male and female cynomolgus monkeys (*Macaca fascicularis*) for the respective organs as previously reported by us and others or those calculated for the brain and lung using their measured volumes were utilized for this calculation [20–22]. The mean organ radiation dose and effective

Maiti *et al. EJNMMI Research*   (2025) 15:57

Page 5 of 9

dose per unit administered radioactivity was calculated using the scaled human time-integrated activity utilizing the program OLINDA/EXM (Organ Level Internal Dose Assessment) version 2.2 for ^{11}C following the adult human male and female anthropomorphic models [20, 22, 23]. Specifically, effective doses were calculated using updated ICRP103 organ weighting factors for radiation quality and organ sensitivity.

Results

Nonhuman primate radioactivity biodistribution

The distribution of radioactivity in the primary target organs at approximately 20 min and 1 h after injection are presented in Table 1.

The non-decay corrected organ time-activity curves obtained from scans in the two male macaques and two separate scan sessions in the same female macaque are illustrated in Fig. 2. The scatter plots were fitted with one or two exponential functions; least square minimization yielded the best fitting parameters. Predominant accumulation of radioactivity (as percentage of the injected dose) was within the liver (~ 40%) and with lower levels in the lungs (~ 12%), heart (~ 5%), spleen (~ 3%) and brain (~ 3%). Localization of radioactivity in the brain was notable for selective uptake in the striatum (Fig. 2s). Low accumulation occurred in the kidneys and urinary bladder. Gradual clearance from the organs were noted except from the heart, lungs and spleen that had faster clearance closely reflecting the clearance from the blood compartment. The time course of activity in the remainder of the body represents the sum of activity in blood not specifically assigned to any organ as well as the non-selective distribution throughout the body. The average values of

the time-integrated activity obtained from the two males and two separate scans from the same female are shown in Table 2; the relatively low standard deviations except for the gallbladder demonstrate good reproducibility.

Table 3 shows the results of the OLINDA/EXM 2.2 organ radiation dose estimations of [11C]TZ1964B based on the time-integrated activity for the human adult male and female model.

The individual organ radiation dose estimates account for organ self-irradiation as well as the fraction attributable to external radiation from source organs in close proximity. The liver, spleen and gallbladder received the highest doses. None of the organs received a radiation burden exceeding 53.3 μGy/MBq. The effective dose for [11C]TZ1964B was 5.02 μSv/MBq in male and 5.84 μSv/MBq in female (Table 4).

Discussion

The accurate assessment of the absorbed radiation dosimetry of [11C]TZ1964B is an important preliminary step before translation to clinical applications of this PET radiopharmaceutical. The extrapolated human dosimetry measures from the PET based measurements of absorbed radioactivity in nonhuman primates after intravenous administration of [11C]TZ1964B is reported here. The principal findings in addition to the selective striatal uptake previously reported by our group [15, 16] were the widespread biodistribution of the radiotracer with liver being the critical organ and the relatively low exposure to radiosensitive organs; the gradual clearance from the liver and accumulation in the gallbladder were suggestive of hepatobiliary clearance.

Table 2 Organ time-integrated activity in nonhuman primates

Organ	Time-integrated activity[a] (h)	Time-integrated activity[a] (h)
	Mean and individual measures in two male macaques [Mean (male#1), (male#2)]	Mean and individual measures in two scans in the same female macaque [Mean; (scan#1), (scan#2)]
Brain	0.011 (0.006, 0.015)	0.009 (0.008, 0.009)
Lungs	0.027 (0.020, 0.035)	0.017 (0.011, 0.024)
Heart wall	0.008 (0.007, 0.009)	0.006 (0.004, 0.007)
Heart contents	0.0005 (0.0003, 0.0008)	0.0003 (0.0001, 0.0004)
Spleen	0.009 (0.0095, 0.0078)	0.017 (0.0143, 0.0192)
Liver	0.253 (0.319, 0.186)	0.208 (0.187, 0.229)
Gallbladder	0.0007 (0.0007, 0.0006)	0.006 (0.0028, 0.0088)
Kidney	0.011 (0.0103, 0.0122)	0.008 (0.0020, 0.0138)
Bladder	0.0019 (0.0007, 0.0032)	0.0005 (0.0002, 0.0007)
Intestine	0.001 (0.0009, 0.0013)	0.002 (0.0019, 0.0016)
Remainder-of-body	0.167 (0.115, 0.219)	0.217 (0.259, 0.176)

[a] Time-integrated activity presented here are the calculated measures in nonhuman primates before extrapolation to human estimates

Table 3 Extrapolated human radiation dose estimates for [^{11}C]
TZ1964B

Target organ	Males (µGy/MBq)	Females (µGy/MBq)
Adrenals	8.95	11.17
Brain	4.38	4.22
Breasts		2.09
Esophagus	3.77	4.72
Eyes	1.01	1.61
Gallbladder wall	13.30	35.85
Left colon	2.19	3.15
Small intestine	2.29	3.73
Stomach wall	3.59	4.21
Right colon	3.70	3.74
Rectum	1.11	1.82
Heart wall	10.95	8.93
Kidneys	11.50	11.92
Liver	*53.25*	*52.90*
Lungs	7.38	5.99
Ovaries		2.01
Pancreas	4.35	7.09
Prostate	1.22	
Salivary glands	1.15	1.69
Red marrow	1.91	2.42
Osteogenic cells	1.47	1.93
Spleen	15.75	35.35
Testes	0.78	
Thymus	2.40	2.78
Thyroid	1.52	1.93
Urinary bladder wall	1.82	1.81
Uterus		1.95
Total body	2.41	3.68

Data in italics represent critical organ

A nonhuman primate model of absorbed radiation measures becomes particularly relevant in the setting of hepatic metabolism of the radiotracer, as the gallbladder may receive and accumulate its metabolites and potentially be a critical organ with high radiation burden. In fact, the gradual clearance from the liver was also noted in prior biodistribution study of [^{11}C]TZ1964B in rats[13]. However, rats lack gallbladder making that animal model inadequate for estimating human dose exposure and justifies the choice of nonhuman primates that closely resembles human physiology for this dosimetry analysis.

The liver is indeed the critical organ for [^{11}C]TZ1964B; the tissue biodistribution raises the possibility of in vivo hepatic degradation. The absorbed radiation dose estimates for liver were 53.3 µGy/MBq for males and 52.9 µGy/MBq in females. Other organs with high radiation dose were the gallbladder and spleen, with maximal absorbed radiation dose estimates of 35.9 and 35.4 µGy/MBq respectively. The maximal radiation dose estimate for the heart wall was 10.9 µGy/MBq.

Prior mRNA expression profile of PDE10A demonstrated strikingly selective gene expression in the brain especially in the caudate that was almost 20 fold-higher than multiple peripheral tissues in humans [24]. Of the peripheral tissues, highest levels of PDE10 mRNA was present in the thyroid; with detectable expression levels in kidneys, heart and lungs. The PDE10A expression was significantly lower in other peripheral tissues tested including liver and spleen [24]. Importantly, relatively low exposure to thyroid (1.93 µGy/MBq), a radiosensitive organ was noted in our analysis. The PDE10A expression pattern could account for the relatively high absorbed radiation noted in the heart wall (in addition to the exposure to radioactivity due to high blood volume in the heart chambers) but does not quite explain the relatively high estimates in the liver, gallbladder and spleen. The gradual clearance from the liver and accumulation of the radiotracer in the gallbladder (in the setting of relatively low absorbed radiation in kidneys and lack of accumulation in the bladder) were suggestive of predominantly hepatobiliary clearance rather than renal elimination of this radiotracer. This could potentially contribute to the high radiation dose received by the liver. On the contrary, the rapid clearance from the spleen closely reflected the clearance from the blood compartment and hence the splenic perfusion appears to be largely responsible for the relatively high radiation dose to the spleen. It would also be important to note as elaborated in the Methods section, our approach to generating the spleen VOI s is a very conservative one and likely overestimates the absorbed radiation dose in the spleen. Even though there is selective accumulation in the brain especially in the striatum, the brain overall receives a relatively modest radiation dose (4.4 µGy/MBq), possibly due to the modest partitioning of the compound into the brain. Radiation dose estimates for the kidneys (11.9 µGy/MBq) and urinary bladder (1.8 µGy/MBq) argue against predominant renal clearance of [^{11}C]TZ1964B.

Significantly greater (around twice as much) absorbed radiation dose estimate for the gallbladder were noted in female compared to males. While pharmacologic (e.g. dosage of ketamine, glycopyrrolate with anticholinergic properties, time interval between tracer injection and induction of anesthesia etc.) and non-pharmacologic (duration of starvation, variances in diet) factors could contribute to such discrepancy, close scrutiny did not reveal significant differences in any of these confounding variables across studies. Of note, the female macaque received ondansetron (5HT3 receptor antagonist) during

Maiti *et al. EJNMMI Research*   (2025) 15:57

Page 7 of 9

Table 4 Summary Table with effective dose for human radiation dose estimates for [¹¹C]TZ1964B

Macaques	Age	Sex	Weight (kg)	Injected activity (MBq)	Injected mass (µg)	Effective dose (µSv/MBq)
Male#1	7y9mo	Male	8.6	302.3	0.15	5.42
Male#2	8y2mo	Male	6.8	336.3	0.26	4.62
Female-scan#1	7y9mo	Female	6.9	342.3	0.08	6.43
Female-scan#2	10y9mo	Female	7.8	384.4	0.79	5.25
Effective dose[a] (µSv/MBq)	5.02 (Male)	5.84 (Female)				
Mean effective dose[a] (µSv/MBq)	5.43					

[a] Effective doses reported here were calculated using updated ICRP103 organ weighting factors The same female monkey was scanned twice at 3 years interval

scan session#2 due to emesis after induction of anesthesia. Ondansetron was not administered in any of the other animals during the scan sessions. Although the data is not entirely clear, limited evidence in the literature suggests ondansetron could inhibit gallbladder emptying [25, 26] and this may have contributed to the enhanced accumulation of radioactivity in the gallbladder (time-activity curve from scan#2 in the female (Fig. 2) demonstrated continued accumulation of radiotracer up to around 170 min) well in excess of what was evidenced in scan session#1 in the same female monkey. Speculatively, significantly greater age at the time of scan#2 (Table 4) obtained 3 years later, could also have potentially contributed to the variances in the gallbladder uptake between scan sessions from the same female. However, even the larger dose calculation still is substantially below guidelines for non-radiosensitive organs. Furthermore, different calculations for gallbladder uptake make almost no differences in the effective dose estimates. Similarly, almost two times higher time-integrated activity and radiation dose estimates were evidenced for the spleen in the female compared to the males. Unlike the gallbladder however, there was significant concordance between the two scans in the same female macaque obtained 3 years apart. Any definitive inferences regarding significant sex differences are precluded by the fact that the same female monkey was scanned twice in the current study. This could be a unique physiological variance in this particular macaque. A much larger "n" could potentially clarify the differences across sexes reported here but this is not the goal of the current dosimetry analysis. More importantly this study demonstrates the significantly greater measures in the female are also well and truly within the allowed absorbed dose limits.

For a maximum absorbed dose of 50 mSv to the critical organ as per FDA 21 CFR 371.1 regulations (< 50 mSv to any organ, < 30 mSv to radiation sensitive organs), our estimates indicate that doses up to 938 MBq of [¹¹C]TZ1964B can be administered to human subjects. The relatively low exposure to the radiosensitive organs including bone marrow, thyroid, gonads etc. (all calculated absorbed doses < 2.5 mSv) safely permits this total injected dose.

Due to its shorter half-life, [¹¹C]TZ1964B could be utilized for multiple scans in the same subject on the same day. Given the liver is a critical organ, it becomes imperative to exercise caution when combining with another radiopharmaceutical with predominantly hepatobiliary clearance. The effective dose for [¹¹C]TZ1964B closely resembled the mean effective dose of 21 other ¹¹C-labeled tracers (range 3.0–6.8 µSv/MBq) [27]. Importantly however, close scrutiny of nine ¹¹C-labeled tracers with available dosimetry analyses in monkeys and

Maiti *et al. EJNMMI Research*   (2025) 15:57

Page 8 of 9

humans, the effective dose extrapolated from monkeys (7.3 ± 1.6 μSv/MBq) were generally noted to overestimate the actual measured effective dose in humans (5.7 ± 1.2 μSv/MBq) and monkeys had a higher liver uptake[27]. This sets the stage for further human PET studies with [^{11}C]TZ1964B to sort out these issues including the sex-differences reported here.

Conclusions

The absorbed radiation dosimetry exposure in humans associated with the intravenous injection of [^{11}C]TZ1964B was determined by whole body PET imaging in primates and extrapolation utilizing OLINDA calculation methods. The critical organ was the liver (53.3 μGy/MBq for males and 52.9 μGy/MBq for females) with high dose also to gallbladder (35.9 μGy/MBq) and spleen (35.4 μGy/MBq). The effective doses were calculated as 5.02 and 5.84 μSv/MBq for males and females, respectively with a mean effective dose of 5.4 μSv/MBq. Given the relatively low exposure to radiosensitive organs, this study proposes that doses up to 938 MBq of [^{11}C]TZ1964B can be safely administered to human subjects for PET measurements of PDE10A activity.

Abbreviations

PDE10A	phosphodiesterase10A
PET	Positron emission tomography
VOI	volume of interest
MSN	medium spiny neuron
cAMP	cyclic AMP
PKA	protein kinase A
HPLC	high-performance liquid chromatography

Supplementary Information

The online version contains supplementary material available at https://doi.org/10.1186/s13550-025-01221-x.

> Supplementary material 1I could not download this even after multiple attempts.

Declarations

Ethics approval and consent to participate

This article does not contain any studies with human participants performed by any of the authors. We used the minimum number of animals necessary for this study, and in accordance with the recommendations of the Weatherall report "The use of non-human primates in research," and took all steps to ameliorate suffering in our studies. Guidelines prescribed by the National Institutes of Health (NIH) Guide for the Care and Use of Laboratory Animal were followed, and this work had the approval the Institutional Animal Care and Use Committee (IACUC; study numbers: 20150166 and 20180143) at Washington University in St. Louis. All animals were housed individually; maintained in facilities with 12-h dark and light cycles; provided access to food and water ad libitum; and were equally engaged with a variety of psychologically-enriching tasks, such as watching movies or playing with appropriate toys.

Consent for publication

Not applicable.

Competing Interests

The authors declare that they have no competing interests.

Author details

^{1}Department of Neurology, Washington University School of Medicine, St. Louis, MO, USA. ^{2}Department of Radiology, Washington University School of Medicine, St. Louis, MO, USA. ^{3}Program in Physical Therapy, Washington University School of Medicine, St. Louis, MO, USA. ^{4}Program in Occupational Therapy, Washington University School of Medicine, St. Louis, MO, USA. ^{5}Department of Neuroscience, Washington University School of Medicine, St. Louis, MO, USA.

References

1. Kotera J, Fujishige K, Yuasa K, Omori K. Characterization and phosphorylation of PDE10A2, a novel alternative splice variant of human phosphodiesterase that hydrolyzes cAMP and cGMP. Biochem Biophys Res Commun. 1999;261:551–7. https://doi.org/10.1006/bbrc.1999.1013.
2. Liu H, Jin H, Luo Z, Yue X, Zhang X, Flores H, et al. In Vivo Characterization of Two (18)F-Labeled PDE10A PET Radioligands in Nonhuman Primate Brains. ACS Chem Neurosci. 2018;9:1066–73. https://doi.org/10.1021/acschemneuro.7b00458.
3. Nishi A, Kuroiwa M, Miller DB, O'Callaghan JP, Bateup HS, Shuto T, et al. Distinct roles of PDE4 and PDE10A in the regulation of cAMP/PKA signaling in the striatum. J Neurosci Offic J Soc Neurosci. 2008;28:10460–71. https://doi.org/10.1523/JNEUROSCI.2518-08.2008.
4. Menniti FS, Faraci WS, Schmidt CJ. Phosphodiesterases in the CNS: targets for drug development. Nat Rev Drug Discov. 2006;5:660–70. https://doi.org/10.1038/nrd2058.

Maiti *et al. EJNMMI Research*   (2025) 15:57

Page 9 of 9

5. Kehler J, Nielsen J. PDE10A inhibitors: novel therapeutic drugs for schizophrenia. Curr Pharm Des. 2011;17:137–50. https://doi.org/10.2174/13816 1211795049624.
6. Bender AT, Beavo JA. Cyclic nucleotide phosphodiesterases: molecular regulation to clinical use. Pharmacol Rev. 2006;58:488–520. https://doi.org/10.1124/pr.58.3.5.
7. Hebb AL, Robertson HA, Denovan-Wright EM. Striatal phosphodiesterase mRNA and protein levels are reduced in Huntington's disease transgenic mice prior to the onset of motor symptoms. Neuroscience. 2004;123:967–81. https://doi.org/10.1016/j.neuroscience.2003.11.009.
8. Russell DS, Barret O, Jennings DL, Friedman JH, Tamagnan GD, Thomae D, et al. The phosphodiesterase 10 positron emission tomography tracer, [18F]MNI-659, as a novel biomarker for early Huntington disease. JAMA Neurol. 2014;71:1520–8. https://doi.org/10.1001/jamaneurol.2014.1954.
9. Russell DS, Jennings DL, Barret O, Tamagnan GD, Carroll VM, Caille F, et al. Change in PDE10 across early Huntington disease assessed by [18F]MNI-659 and PET imaging. Neurology. 2016;86:748–54. https://doi.org/10.1212/WNL.0000000000002391.
10. Tu Z, Fan J, Li S, Jones LA, Cui J, Padakanti PK, et al. Radiosynthesis and in vivo evaluation of [11C]MP-10 as a PET probe for imaging PDE10A in rodent and non-human primate brain. Bioorg Med Chem. 2011;19:1666–73. https://doi.org/10.1016/j.bmc.2011.01.032.
11. Celen S, Koole M, Ooms M, De Angelis M, Sannen I, Cornelis J, et al. Preclinical evaluation of [(18)F]JNJ42259152 as a PET tracer for PDE10A. Neuroimage. 2013;82:13–22. https://doi.org/10.1016/j.neuroimage.2013.04.123.
12. Lin SF, Labaree D, Chen MK, Holden D, Gallezot JD, Kapinos M, et al. Further evaluation of [11C]MP-10 as a radiotracer for phosphodiesterase 10A: PET imaging study in rhesus monkeys and brain tissue metabolite analysis. Synapse. 2015;69:86–95. https://doi.org/10.1002/syn.21792.
13. Fan J, Zhang X, Li J, Jin H, Padakanti PK, Jones LA, et al. Radiosyntheses and in vivo evaluation of carbon-11 PET tracers for PDE10A in the brain of rodent and nonhuman primate. Bioorg Med Chem. 2014;22:2648–54. https://doi.org/10.1016/j.bmc.2014.03.028.
14. Li J, Jin H, Zhou H, Rothfuss J, Tu Z. Synthesis and in vitro biological evaluation of pyrazole group-containing analogues for PDE10A. Medchemcomm. 2013;4:443–9. https://doi.org/10.1039/C2MD20239E.
15. Liu H, Jin H, Yue X, Zhang X, Yang H, Li J, et al. Preclinical evaluation of a promising C-11 labeled PET tracer for imaging phosphodiesterase 10A in the brain of living subject. Neuroimage. 2015;121:253–62. https://doi.org/10.1016/j.neuroimage.2015.07.049.
16. Liu H, Jin H, Yue X, Han J, Yang H, Flores H, et al. Comparison of [(11)C]TZ1964B and [(18)F]MNI659 for PET imaging brain PDE10A in nonhuman primates. Pharmacol Res Perspect. 2016;4: e00253. https://doi.org/10.1002/prp2.253.
17. Takano A, Stepanov V, Gulyas B, Nakao R, Amini N, Miura S, et al. Evaluation of a novel PDE10A PET radioligand, [(11) C]T-773, in nonhuman primates: brain and whole body PET and brain autoradiography. Synapse. 2015;69:345–55. https://doi.org/10.1002/syn.21821.
18. Barret O, Thomae D, Tavares A, Alagille D, Papin C, Waterhouse R, et al. In vivo assessment and dosimetry of 2 novel PDE10A PET radiotracers in humans: 18F-MNI-659 and 18F-MNI-654. J Nucl Med. 2014;55:1297–304. https://doi.org/10.2967/jnumed.113.122895.
19. Antenor-Dorsey JA, Laforest R, Moerlein SM, Videen TO, Perlmutter JS. Radiation dosimetry of N-([11C]methyl)benperidol as determined by whole-body PET imaging of primates. Eur J Nucl Med Mol Imaging. 2008;35:771–8. https://doi.org/10.1007/s00259-007-0644-6.
20. Karimi M, Tu Z, Yue X, Zhang X, Jin H, Perlmutter JS, et al. Radiation dosimetry of [(18)F]VAT in nonhuman primates. EJNMMI Res. 2015;5:73. https://doi.org/10.1186/s13550-015-0149-4.
21. Drevon-Gaillot E, Perron-Lepage MF, Clement C, Burnett R. A review of background findings in cynomolgus monkeys (Macaca fascicularis) from three different geographical origins. Exp Toxicol Pathol. 2006;58:77–88. https://doi.org/10.1016/j.etp.2006.07.003.
22. Stabin MG, Sparks RB, Crowe E. OLINDA/EXM: the second-generation personal computer software for internal dose assessment in nuclear medicine. J Nucl Med. 2005;46:1023–7.
23. Fisher DR, Fahey FH. Appropriate use of effective dose in radiation protection and risk assessment. Health Phys. 2017;113:102–9. https://doi.org/10.1097/HP.0000000000000674.
24. Lakics V, Karran EH, Boess FG. Quantitative comparison of phosphodiesterase mRNA distribution in human brain and peripheral tissues. Neuropharmacology. 2010;59:367–74. https://doi.org/10.1016/j.neuropharm.2010.05.004.
25. Fiorucci S, Santucci L, Morelli A. 5-hydroxytryptamine 3-receptor antagonist modulates gallbladder emptying and motilin release induced by erythromycin. Dig Dis Sci. 1993;38:2236–40. https://doi.org/10.1007/BF01299902.
26. Itoh Z, Mizumoto A, Iwanaga Y, Yoshida N, Torii K, Wakabayashi K. Involvement of 5-hydroxytryptamine 3 receptors in regulation of interdigestive gastric contractions by motilin in the dog. Gastroenterology. 1991;100:901–8. https://doi.org/10.1016/0016-5085(91)90262-j.
27. Zanotti-Fregonara P, Innis RB. Suggested pathway to assess radiation safety of 11C-labeled PET tracers for first-in-human studies. Eur J Nucl Med Mol Imaging. 2012;39:544–7. https://doi.org/10.1007/s00259-011-2005-8.

Publisher's Note